RSC Advances

PAPER

View Article Online
View Journal | View Issue

Cite this: *RSC Adv.*, 2026, **16**, 18166

Sodium alginate-derived hydrophilic Gel@CuO microspheres: a green nanocatalyst for diverse Petasis transformations with antibacterial activity

Nilesh T. Pandit,[a] Avdhut D. Kadam,[a] Avinash A. Survase,[b] Komal R. Mali,[c] Vishvanath B. Ghanwat,[a] Sarika P. Patil,[de] Chaitali S. Bagade,[c] Tukaram D. Dongale[fg] and Santosh B. Kamble *[de]

A sustainable heterogeneous catalytic system based on sodium alginate-derived Gel@CuO microspheres has been developed for Petasis multicomponent reactions under environmentally benign conditions. CuO nanoparticles synthesized *via* a biogenic route using *Buchanania lanzan Spreng* leaf extract were immobilized within a calcium-crosslinked alginate matrix to afford a mechanically robust and hydrophilic microsphere nanocatalyst. Comprehensive characterization by FT-IR, XRD, SEM-EDX, XPS, TGA-DTA, and contact angle analysis confirmed successful CuO entrapment, uniform elemental distribution, strong metal–polymer interactions, and high thermal stability. The Gel@CuO nanocatalyst enabled the synthesis of 27 structurally diverse Petasis products, delivering isolated yields of 86–99% within 7–90 min in an aqueous sodium *p*-toluenesulfonate (NaPTS) hydrotropic medium under mild conditions. Quantitative green metrics revealed low total PMI values (9.2–14.1 g g^{-1}) and high Reaction Mass Efficiency (RME = 77–85%) for alkylaminophenol derivatives, while more complex substrates showed moderately higher PMI yet retained excellent yields. The catalyst exhibited excellent recyclability over multiple cycles with negligible activity loss. In addition, the Gel@CuO microspheres displayed notable antibacterial activity against both Gram-positive (*Staphylococcus aureus, Bacillus cereus*) and Gram-negative (*Salmonella typhimurium, Proteus vulgaris*) bacteria. Overall, this work presents a biopolymer-based, recyclable nanocatalyst offering a sustainable platform for organic transformation.

Received 3rd February 2026
Accepted 30th March 2026

DOI: 10.1039/d6ra00921b

rsc.li/rsc-advances

1 Introduction

Multicomponent reactions (MCRs) play a pivotal role in modern synthetic chemistry due to their inherent atom economy, operational simplicity, and ability to rapidly assemble molecular complexity in a single step.[1,2] Among these, the Petasis reaction, also known as the borono-Mannich reaction, has emerged as a powerful strategy for constructing C–C and C–N bonds using amines, carbonyl compounds, and organoboron reagents.[3,4] This transformation provides access to structurally diverse scaffolds such as alkylaminophenols,[5] aryl-glycines,[6] and fused heterocycles,[7] many of which exhibit significant biological and pharmaceutical relevance. Despite its utility, traditional Petasis methodologies frequently rely on organic solvents, long reaction times, and stoichiometric promoters, which limit their sustainability and applicability under green chemistry conditions. To address these challenges, numerous catalytic systems, including Brønsted acids, metal salts, and homogeneous Lewis acids,[8] have been explored. However, such catalysts often suffer from drawbacks, including poor recyclability, catalyst leaching, handling difficulties, and incompatibility with aqueous media. Consequently, there remains a pressing need for robust, heterogeneous, eco-friendly, and easily recoverable catalysts capable of efficiently driving Petasis transformations, particularly in aqueous or hydrotropic environments.

Copper oxide nanoparticles (CuO NPs) are attractive candidates in this context owing to their low cost, abundance, and strong Lewis acidic nature.[9] CuO-based nanomaterials have demonstrated efficacy in numerous C–N, C–O, and C–C bond-forming reactions. However, their practical use is often hindered by a tendency to aggregate, reduced surface accessibility, and poor reusability under reaction conditions. Immobilizing or entrapping CuO nanoparticles within a stable

[a]*Department of Chemistry, Yashavantrao Chavan Institute of Science, Constituent College, Karmaveer Bhaurao Patil University, Satara-415001, Maharashtra, India*
[b]*Department of Microbiology, Yashavantrao Chavan Institute of Science, Constituent College, Karmaveer Bhaurao Patil University, Satara-415001, Maharashtra, India*
[c]*Department of Chemistry, Shivaji University Kolhapur, Maharashtra, India*
[d]*Department of Chemistry, Sadguru Gadage Maharaj College, Karad-415124, Maharashtra, India. E-mail: santosh.san143@gmail.com*
[e]*Karmaveer Bhaurao Patil University, Satara-415001, Maharashtra, India*
[f]*School of Nanoscience and Biotechnology, Shivaji University, Kolhapur-416004, Maharashtra, India*
[g]*School of Electrical Engineering, Korea University, Anam-ro 145, Seongbuk-gu, Seoul, Republic of Korea*

support can overcome these limitations by preventing agglomeration and enhancing catalyst stability. In recent years, plant-mediated synthesis of metal oxide nanoparticles has emerged as a sustainable alternative to conventional chemical routes.[6,10,11] In this context, *Buchanania lanzan Spreng* (family: Anacardiaceae), a medicinally important tree commonly known as charoli, serves as an excellent bio-resource.[12] Its leaves are rich in phenolics (*e.g.*, gallic acid), flavonoids (*e.g.*, rutin, quercetin), tannins, saponins, phenolic acids, steroids, alkaloids, and antioxidant compounds capable of acting simultaneously as reducing, stabilizing, and capping agents during nanoparticle formation.[13,14] These biomolecules possess functional groups such as hydroxyl and carbonyl groups and are widely known for their reducing, stabilizing, and antioxidant properties.[15] The presence of these phytoconstituents contributes to the biological and chemical activity of the plant and makes the extract a valuable natural source of bioactive compounds. These phytoconstituents facilitate the mild and eco-friendly conversion of copper precursors into CuO nanoparticles without the need for toxic reducing agents or harsh reaction conditions. The resulting green CuO nanoparticles possess abundant surface functional groups that improve dispersibility and interaction with polymeric matrices, making them ideal candidates for incorporation into biopolymer-based catalytic systems.

In addition to catalyst design and reaction conditions, the electronic nature of substituents present on the aldehyde and boronic acid components plays a crucial role in determining the efficiency of the Petasis reaction. Electron-donating groups on boronic acids generally enhance the nucleophilicity and migratory aptitude of the aryl group, thereby facilitating the key C–C bond-forming step. Similarly, substituents on salicylaldehyde derivatives influence the formation and stability of the iminium ion intermediate as well as the coordination ability of the phenolic oxygen with the catalytic metal centre. In contrast, strongly electron-withdrawing groups may reduce electron density and slow down the reaction rate. Therefore, understanding the structure–reactivity relationship governed by functional group effects is essential for optimizing reaction efficiency and expanding substrate scope in catalytic Petasis transformations. The general reaction for the Petasis reaction investigated in this study is shown in Scheme 1.

Sodium alginate, a renewable, biodegradable polysaccharide extracted from brown algae, has recently gained attention as a green support material for immobilizing the nanocatalysts.[16] Alginate undergoes rapid gelation in the presence of divalent cations such as Ca^{2+} through the well-known "egg-box" cross-linking mechanism,[17,18] producing hydrogels with high porosity, excellent mechanical stability, and a 3D network ideal for nanoparticle entrapment.[19] Such biopolymer-derived gels are non-toxic, inexpensive, water-processable, and environmentally benign, making them attractive alternatives to conventional inorganic supports.[20,21] Despite their potential, alginate-based catalyst systems have not been investigated for Petasis reactions, and no report exists on the use of alginate-entrapped CuO for multicomponent transformations.

Hydrotropic media such as sodium *p*-toluenesulfonate (NaPTS) further enhance the green nature of these transformations by increasing substrate solubility, suppressing side reactions, and enabling metal-catalyzed reactions under mild, aqueous conditions.[22] Combining hydrotropy with a recyclable biopolymer-based nanocatalyst offers an attractive and sustainable strategy for Petasis chemistry.

Herein, the main objective of this study is to develop a sustainable, efficient, and recyclable heterogeneous nanocatalyst based on sodium alginate-derived Gel@CuO microspheres for promoting Petasis multicomponent reactions under green aqueous conditions. In this context, we present the first sodium-alginate-derived Gel@CuO microspheres incorporating *Buchanania lanzan*-mediated green CuO nanoparticles, serving as a recyclable, water-compatible heterogeneous nanocatalyst for diverse Petasis transformations. The CuO nanoparticles are uniformly entrapped within a calcium-crosslinked alginate microsphere nanocatalyst, forming a stable 3D network that inhibits nanoparticle agglomeration while maintaining high catalytic accessibility. The Gel@CuO nanocatalyst efficiently promotes the synthesis of alkylaminophenols (entries 1–22), indoline-derived aryl-glycines (entries 23–24), and fused morpholine–pyrrolidines (entries 25–27) under mild aqueous NaPTS conditions with excellent yields, short reaction times, and outstanding recyclability. Green chemistry metrics further support the sustainability of this methodology, as evidenced by low total PMI values, high reaction mass efficiency (RME), and favorable atom economy across the product series. The use of aqueous hydrotropic media, minimal solvent waste, and a recyclable heterogeneous catalyst collectively contribute to reduced environmental impact and improved process efficiency. This study demonstrates a sustainable platform that merges green synthesis, biopolymer engineering, and catalysis to deliver an efficient and environmentally benign Petasis reaction protocol.

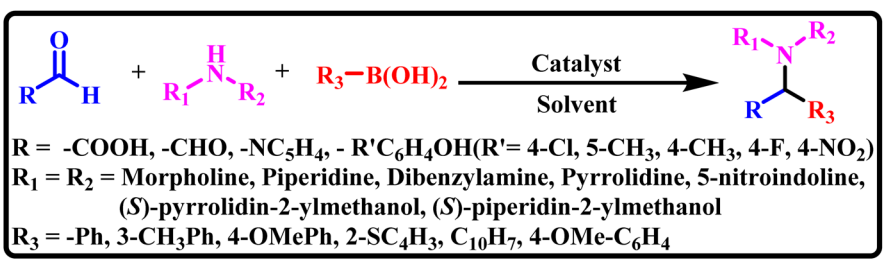

Scheme 1 General reaction scheme for the Petasis reaction.

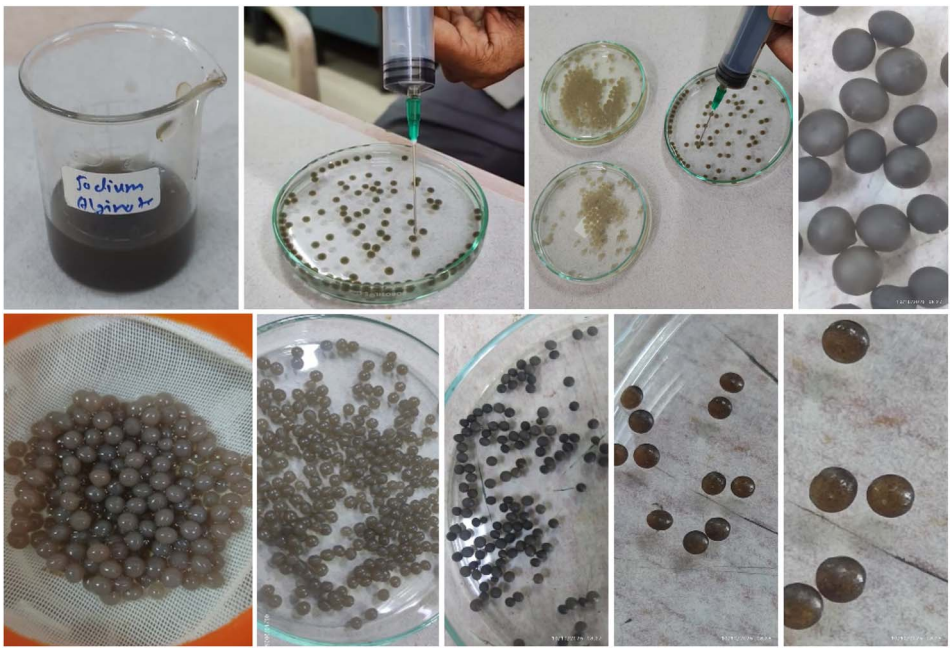

Fig. 1 Visual representation of the synthesis process of Gel@CuO microspheres, including alginate–CuO mixing, syringe-assisted droplet formation, $CaCl_2$ crosslinking, washing, and final dried microspheres.

2 Experimental

2.1 Materials and reagents

2.1.1 Reagents. All reagents and chemicals employed in this work, including sodium alginate, copper acetate, calcium chloride, boronic acids, aldehydes and amines, were of analytical reagent grade and obtained from Sigma-Aldrich. They were used as received without any additional purification, and double-distilled water was utilized throughout all synthesis procedures.

2.1.2 Preparation CuO NPs. CuO nanoparticles were synthesized *via* a green route using a modified version of a reported methodology.[6,19] The leaf extract of *Buchanania lanzan Spreng* was prepared using a Soxhlet extraction system. An aqueous solution of copper acetate (0.05 M, 50 mL) was prepared in distilled water, and 25 mL of the plant extract was introduced into this solution under ultrasonic probe irradiation to initiate complexation. Subsequently, 25 mL of 1.0 M KOH was added dropwise under continued ultrasonication to induce precipitation of the copper precursor. The reaction mixture was further sonicated for 30 min to ensure the complete formation of CuO nanostructures.

The resulting suspension was centrifuged, and the solid product was collected, washed, and dried at room temperature. The dried material was then calcined at 300 °C for 2 h to obtain phase-pure green-synthesized CuO nanoparticles. The resulting CuO NPs were characterized using standard analytical techniques and subsequently employed for entrapment within the alginate gel matrix.

2.1.3 Preparation of gel-entrapped CuO NPs. Gel-entrapped CuO NPs were prepared using the modified reported methodology.[23] Sodium alginate (0.40 g) was dissolved in 10 mL of distilled water in a clean 50 mL beaker with gentle heating until a homogeneous viscous solution was obtained. In a separate 50 mL beaker, CuO nanoparticles (0.15 g) were dispersed in 10 mL of distilled water by ultrasonication to ensure uniform suspension. The CuO dispersion was then added to the cooled sodium alginate solution and mixed thoroughly using a glass rod, followed by gentle heating to obtain a consistent gel precursor mixture.

For microspheres formation, a 5 mL syringe (selected based on the desired microspheres size) was used to drop the alginate–CuO mixture into a 2.8 g $CaCl_2$ solution prepared in 40 mL of distilled water. Upon contact with the $CaCl_2$ solution, the droplets instantly formed solid Gel@CuO microspheres through ionic crosslinking. The microspheres were allowed to harden for 20 minutes, collected by filtration, and initially dried at ambient temperature. Final drying was performed in an oven at 60 °C, and the dried microspheres were stored in clean glass vials for subsequent catalytic applications. Fig. 1 illustrates the stepwise formation of Gel@CuO microspheres *via* ionic crosslinking of sodium alginate in the presence of Ca^{2+}. The gel-entrapped CuO catalyst were characterized using standard techniques such as XRD, IR, SEM, EDS, XPS, TGA-DTA, and contact angle.

2.2 Instrumentation

A comprehensive set of analytical techniques was used to characterise the synthesized nanocatalyst and its reaction products with respect to structure, morphology, composition, and functional groups. The crystalline phase of the Gel@CuO was verified by X-ray diffraction (XRD) using a BRUKER AXS D8 Advance diffractometer equipped with Cu Kα radiation ($\lambda = 1.54$ Å) operated at 40 kV. Fourier Transform Infrared Spectroscopy

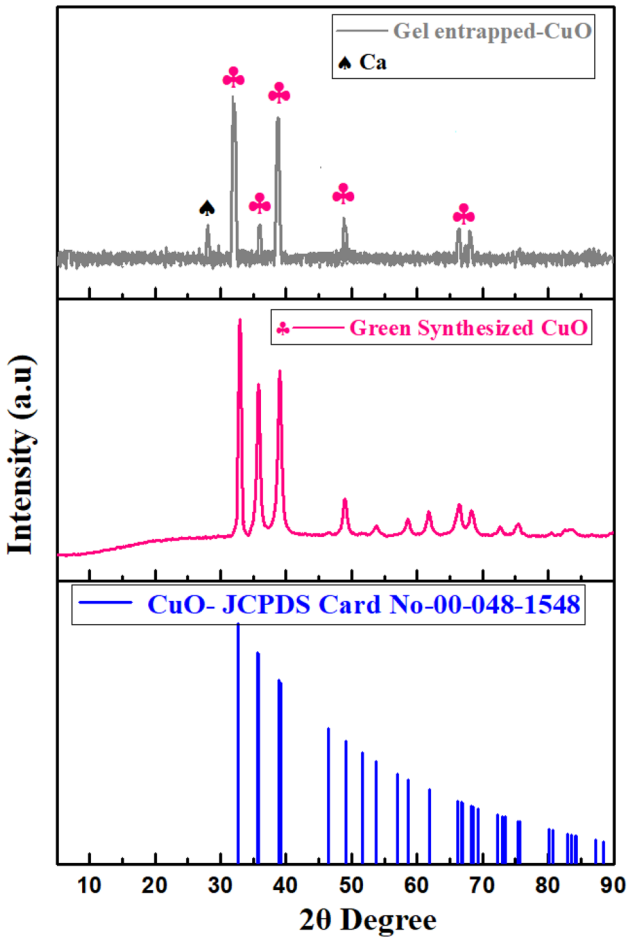

Fig. 2 XRD patterns of green-synthesized CuO and Gel@CuO microspheres, with the reference CuO JCPDS card (No. 00-048-1548), confirm the formation of monoclinic CuO and its successful entrapment within the alginate matrix.

(FT-IR) was performed on a Lambda Scientific FT-IR 7600 instrument to identify characteristic functional groups. Surface features and morphological details were observed using Scanning Electron Microscopy (SEM) with a JEOL JSM-IT200 system, and the elemental composition was further examined *via* Energy-Dispersive X-ray (EDS) spectroscopy attached to the SEM. Structural confirmation of the organic Petasis products was achieved by ^{1}H and ^{13}C Nuclear Magnetic Resonance (NMR) spectroscopy on a Bruker AC 400 MHz instrument (400 MHz for ^{1}H and 100 MHz for ^{13}C), employing $CDCl_3$ as the solvent and tetramethylsilane (TMS) as the internal standard. All obtained spectral and graphical data were processed and visualized using OriginPro 2024 (64 bit) SR1 software. The chemical structures were drawn using ChemDraw 22.0 software.

2.3 Catalytic experiments

2.3.1 Synthesis of alkylaminophenols, indoline-derived arylglycines and fused heterocycle derivatives. A mixture of the amine (1.0 mmol), aldehyde (1.0 mmol), and Gel@CuO microspheres (0.03 g) was added to aqueous NaPTS solution (3 mL) and stirred for 5 min. Subsequently, the corresponding boronic acid was introduced, and the reaction mixture was stirred at room temperature until completion, as monitored by TLC. Upon completion, the reaction mixture was filtered to remove the catalyst, and the filtrate was subjected to standard purification procedures. The isolated products were characterized by ^{1}H and ^{13}C NMR spectroscopy.

2.4 Antimicrobial activity

The microbial cultures in1oculums were prepared in sterile saline water. The nutrient agar plates were used as a medium for bacterial growth. The *S. aureus*, *B. cereus*, *S. typhimurium* and *P. vulgaris* cultures were spread on sterile nutrient agar plates, and wells were prepared in these plates using a sterile corkborer having a size of 5 mm. 100 μg mL^{-1} synthesized material was dispersed in the sterile dimethyl sulfoxide (DMSO) with the help of a micropipette. The plates were incubated at 37 °C for 24 h to test antibacterial activity.[24]

3 Result and discussion

3.1 Synthesis and characterization

3.1.1 Textural properties

3.1.1.1 XRD. XRD analysis was employed to investigate the crystalline structure of the green-synthesized CuO nanoparticles and Gel@CuO, as well as to evaluate their structural stability after immobilization within the alginate matrix (Fig. 2). The diffraction pattern of both samples exhibit well-defined peaks at 2θ values of approximately 32.5°, 35.5°, 38.7°, 38.9°, 46.2°, 48.7°, 53.4°, 58.3°, 61.5°, 65.8°, 66.3°, and 68.1°, which are indexed to the (−110), (002), (111), (200), (−112), (−202), (020), (202), (−113), (022), (−311), and (−220) planes of monoclinic CuO (tenorite), in excellent agreement with JCPDS card No. 00-048-1548. The high intensity and sharpness of these reflections indicate good crystallinity of the CuO nanoparticles. The average crystallite size of the green-synthesized CuO nanoparticles, calculated using the Debye–Scherrer equation, was found to be 11.82 nm, confirming their nanocrystalline nature. The XRD pattern of Gel@CuO microspheres retains all characteristic CuO reflections, confirming that the crystalline structure of CuO remains intact after entrapment within the calcium-crosslinked alginate network. A noticeable decrease in peak intensity and slight broadening are observed, which can be attributed to the amorphous nature of the alginate matrix and partial shielding of CuO crystallites within the polymeric framework. Additional weak features corresponding to calcium species arise from Ca^{2+}-mediated alginate crosslinking. Overall, the XRD results unequivocally confirm the formation of phase-pure monoclinic CuO and its successful immobilization within the alginate microspheres without structural transformation.

3.1.1.2 SEM. The SEM micrographs of the Gel@CuO microspheres are presented in Fig. 3a–f and provide insight into the surface morphology of the prepared nanocatalyst. The low-magnification images (Fig. 3a and b) reveal that the Gel@CuO material possesses an irregular and rough surface morphology typical of calcium-crosslinked alginate gel structures. The microsphere surface appears uneven and porous, which is

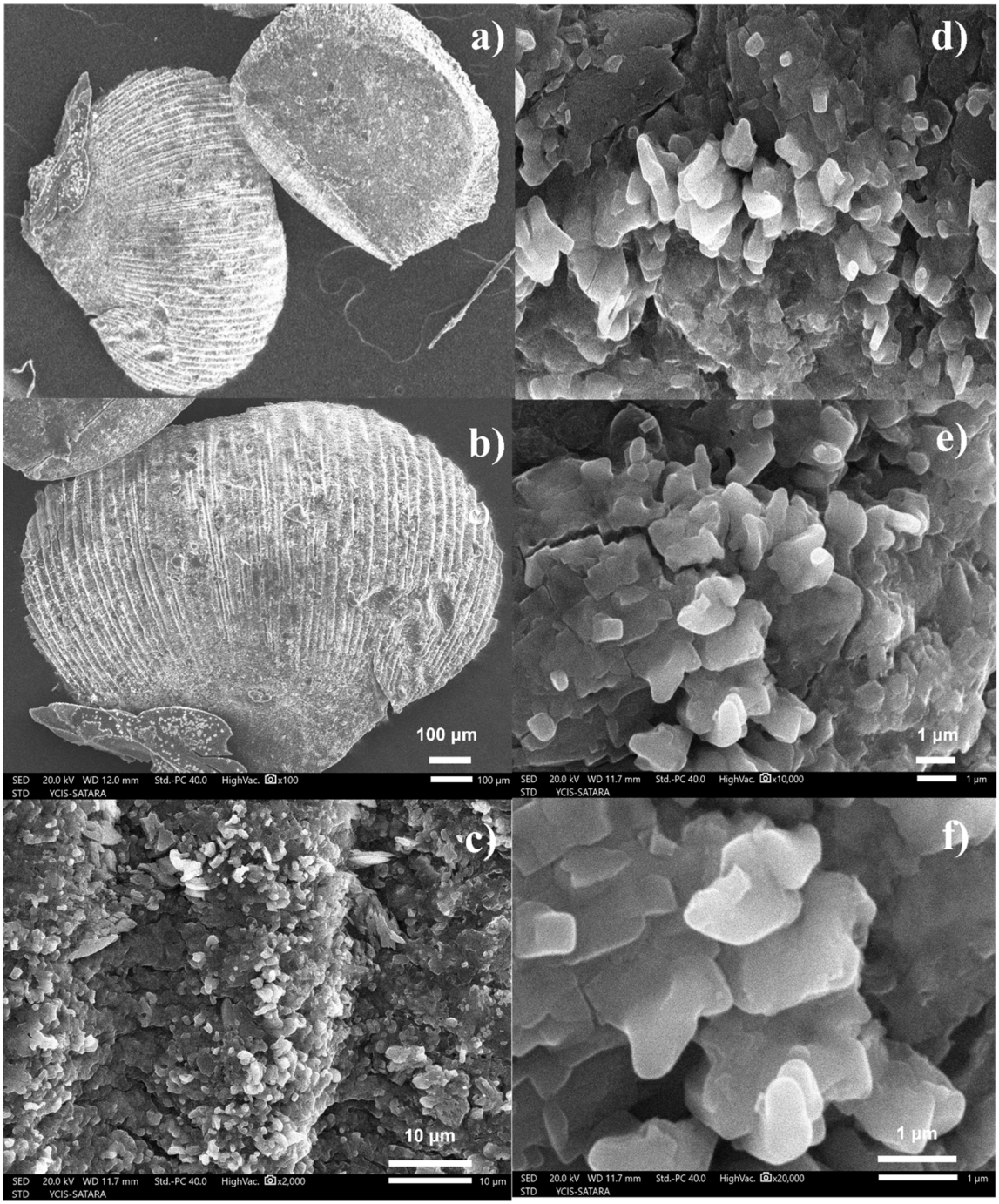

Fig. 3 (a and b): SEM images showing the inner and outer surfaces of Gel@CuO. The outer region displays a rough, ribbed, and porous morphology formed during gel entrapment. (c–f) Magnified SEM micrographs revealing densely packed CuO nanoparticles embedded within the gel matrix, forming irregular, layered, and high-surface-area domains.

consistent with the formation of a polymeric gel network during the Ca^{2+}-induced crosslinking process.

Higher-magnification images (Fig. 3c–f) show the presence of small granular features distributed across the gel surface, which can be attributed to CuO nanoparticles immobilized within the alginate matrix. These particles appear relatively well dispersed within the polymer framework without obvious large-scale aggregation. The rough and heterogeneous surface morphology of the nanocatalyst is expected to provide accessible sites for interaction with reactant molecules during catalytic reactions.

Overall, the SEM observations confirm the successful incorporation of CuO nanoparticles within the alginate gel matrix and the formation of a heterogeneous Gel@CuO microsphere structure suitable for catalytic applications.

3.1.2 Chemical composition

3.1.2.1 FT-IR analysis. Fig. 4 shows the FT-IR spectra recorded for sodium alginate, green-synthesized CuO nanoparticles,

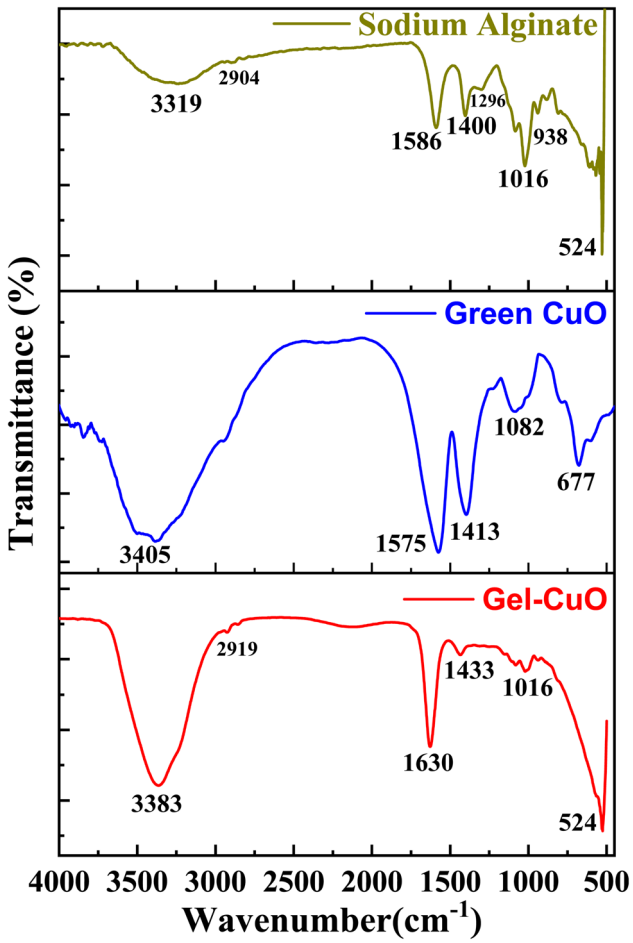

Fig. 4 FT-IR spectra of sodium alginate, green-synthesized CuO nanoparticles, and the Gel@CuO microsphere nanocatalyst, showing characteristic functional groups and confirming successful entrapment of CuO within the alginate matrix.

and the Gel@CuO nanocatalyst. In the spectrum of sodium alginate, a broad absorption band observed at 3319 cm^{-1} corresponds to the stretching vibration of hydroxyl (–OH) groups present in the polysaccharide backbone. Also, the band observed at 2904 is attributed to the C–H stretching present in the polysaccharide backbone. Another band appearing at 1586 cm^{-1} is attributed to the asymmetric stretching vibration of the carboxylate group ($–COO^-$), whereas the band at 1413 cm^{-1} corresponds to the symmetric stretching vibration of $–COO^-$ groups, confirming the presence of carboxylate functionalities in the alginate structure. In addition, the peak at 1082 cm^{-1} is assigned to the stretching vibration of the C–O–C glycosidic linkage in the alginate polysaccharide framework. A weak band around 670 cm^{-1} is also observed, which is associated with skeletal vibrations of the alginate polymer structure.[25]

The FT-IR spectrum of the green-synthesized CuO nanoparticles exhibits a broad band at 3405 cm^{-1}, which corresponds to the stretching vibration of hydroxyl groups arising from surface-adsorbed water molecules or phytochemical residues from the *Buchanania lanzan* leaf extract used during nanoparticle synthesis. The bands at 1586 cm^{-1} and 1400 cm^{-1} are attributed to the stretching vibrations of organic functional groups associated with plant-derived biomolecules acting as reducing and stabilizing agents. Importantly, a characteristic absorption band at 524 cm^{-1} is observed, which corresponds to the Cu–O stretching vibration, confirming the successful formation of copper oxide nanoparticles.[26]

For the Gel@CuO nanocatalyst, the spectrum shows characteristic bands originating from both alginate and CuO components. The broad O–H stretching band appears at 3383 cm^{-1}, while the asymmetric and symmetric stretching vibrations of carboxylate groups are observed at 1630 cm^{-1} and 1433 cm^{-1}, respectively. These shifts compared with pure sodium alginate indicate the replacement of Na^+ ions by Ca^{2+} ions during the ionic crosslinking process, resulting in the formation of a calcium-alginate network. Furthermore, the Cu–O vibration near 524 cm^{-1} remains clearly visible in the Gel@CuO spectrum, demonstrating that the CuO nanoparticles retain their structural integrity after immobilization within the alginate matrix.

3.1.2.2 EDS. The elemental composition of the Gel@CuO microspheres was examined by EDS analysis (Fig. 5). The distinct 8 peaks in the spectrum clearly show the presence of C, O, Ca, Cl, and Cu, which are consistent with the gel matrix and the incorporated CuO nanoparticles. Carbon and oxygen peaks originate primarily from the alginate biopolymer, while calcium and chlorine peaks result from the $CaCl_2$ entrapment process used during microsphere formation. The weak peaks of copper at ~0.9 keV, 8.0 keV, and 8.9 keV confirm the successful incorporation of CuO within the gel network.

The quantitative EDX analysis indicates 38.24 at% C, 41.23 at% O, 13.16 at% Cl, 6.74 at% Ca, and 7.75 at% Cu. Although the surface copper content appears relatively low, this is expected because EDS is a surface-sensitive technique and the outermost alginate layer partially covers the embedded CuO nanoparticles. The detected chlorine content is attributed to residual chloride ions bound within the Ca^{2+}–alginate matrix. The measured elemental profile is consistent with the composition expected from the synthesis procedure, confirming the successful formation of CuO-loaded calcium–alginate microspheres.

The elemental mapping of the Gel@CuO microspheres (Fig. 6) confirms the uniform distribution of all major elements C, O, Ca, Cl, and Cu across the microsphere surface. Carbon and oxygen maps indicate the presence of the alginate polymer matrix, while calcium and chlorine signals correspond to the $CaCl_2$-induced ionic crosslinking. The Cu mapping shows a well-dispersed distribution of CuO nanoparticles throughout the microsphere, with no evidence of aggregation. The combined overlay image further verifies the homogeneous incorporation of CuO within the alginate network, supporting the successful formation of Gel@CuO microspheres.

3.1.2.3 XPS. The XPS analysis (Fig. 7) of the Gel@CuO microspheres confirms the successful incorporation and chemical stability of CuO nanoparticles within the calcium-crosslinked alginate matrix. The survey spectrum exhibits distinct signals corresponding to C, O, Ca, Cl, and Cu, in good agreement with the elemental composition obtained from EDX analysis, thereby validating the uniform distribution of these

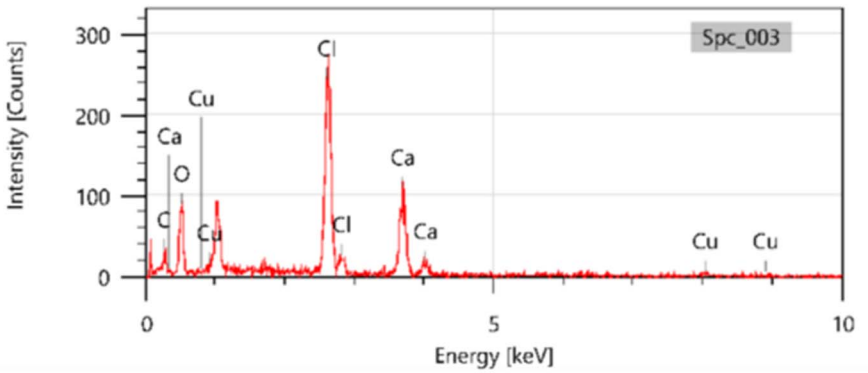

Element	Line	Mass%	Atom%
C	K	24.23±1.18	38.24±1.87
O	K	28.79±1.55	34.11±1.84
Cl	K	24.61±0.62	13.16±0.33
Ca	K	14.26±0.58	6.74±0.27
Cu	K	8.12±0.42	7.75±0.12
Total		100.00	100.00
Spc_003			Fitting ratio 0.2069

Fig. 5 EDS Spectrum of Gel@CuO microspheres.

elements throughout the microspheres. The high-resolution Ca 2p spectrum displays a characteristic peak centered at ~347.3 eV, confirming the presence of Ca^{2+} ions responsible for ionic crosslinking of alginate chains *via* the well-known "egg-box" structure.

The C 1s spectrum shows a dominant peak at 284.56 eV, attributed to C–C/C–H environments, along with contributions from C–O and O–C=O functionalities, indicating that the alginate backbone remains chemically intact after CuO entrapment. The O 1s peak observed at ~531.35 eV arises from overlapping contributions of Cu–O bonds and oxygen-containing functional groups of alginates, reflecting strong interfacial interactions between the inorganic nanoparticles and the biopolymer matrix. Importantly, the Cu 2p spectrum exhibits a Cu $2p_{3/2}$ peak at ~934.36 eV accompanied by characteristic shake-up satellite features, unequivocally confirming that copper exists predominantly in the Cu^{2+} oxidation state, consistent with CuO. The Cl 2p signal at ~198.16 eV is attributed to residual chloride ions originating from $CaCl_2$ used during microsphere formation.

Collectively, the XPS results, in close correlation with EDX findings, unequivocally establish the successful formation of Gel@CuO microspheres with chemically stable, well-dispersed CuO nanoparticles strongly integrated within the calcium-crosslinked alginate network.

3.1.3 Physical properties

3.1.3.1 TGA-DTA. The thermal decomposition profile of the biosynthesized CuO nanoparticles is presented in Fig. 8a. The TGA curve shows three distinct weight-loss regions corresponding to the removal of physically adsorbed species, decomposition of organic residues from the plant extract, and the final conversion into thermally stable CuO. The first weight loss of ~3% occurring below 250 °C is attributed to the evaporation of physically adsorbed moisture and volatile

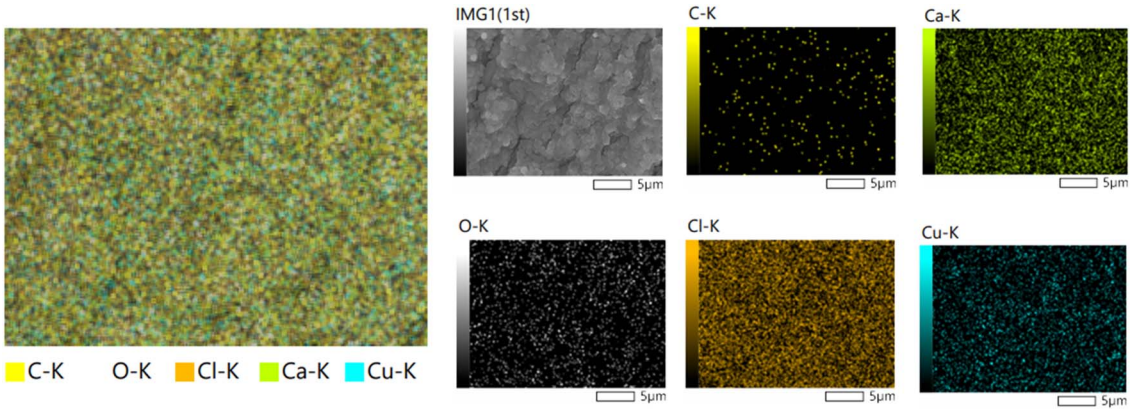

Fig. 6 Elemental mapping of Gel@CuO microspheres showing uniform distribution of C, O, Ca, Cl, and Cu.

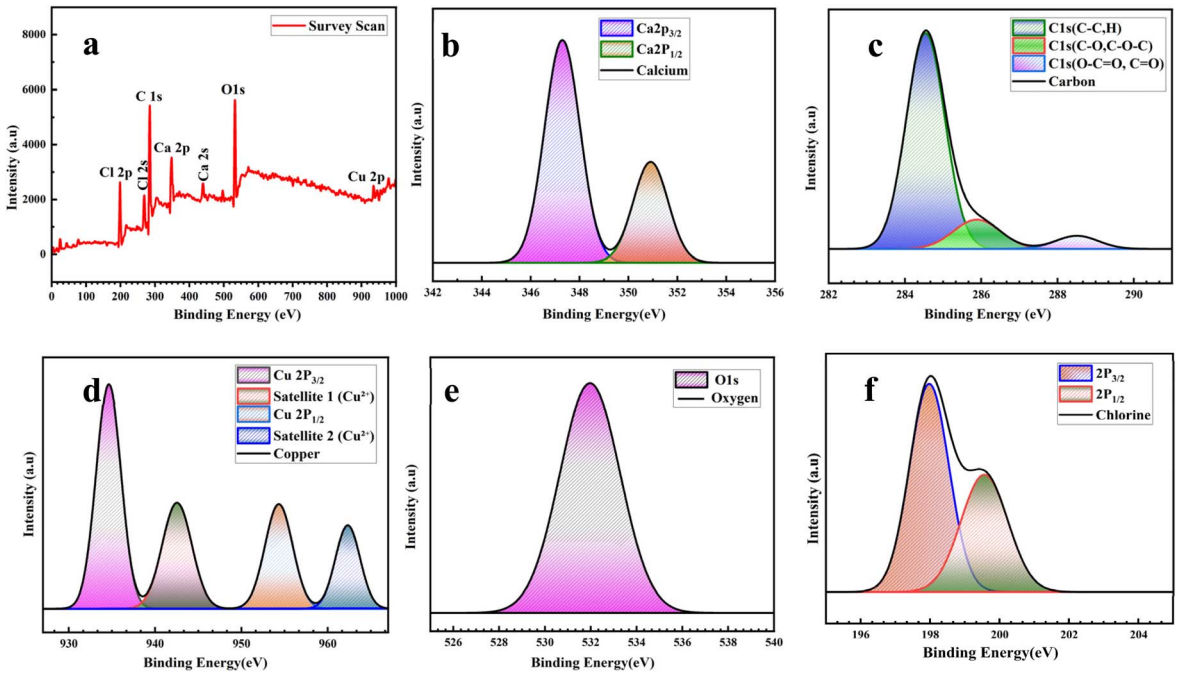

Fig. 7 X-ray photoelectron spectroscopy (XPS) analysis of Gel@CuO microspheres: (a) survey spectrum showing the presence of C, O, Cu, Ca, and Cl elements; (b) high-resolution Ca 2p spectrum; (c) C 1s spectrum; (d) Cu 2p spectrum with characteristic satellite peaks; (e) O 1s spectrum; and (f) Cl 2p spectrum, confirming the chemical composition and successful formation of the Gel@CuO microspheres.

phytoconstituents entrapped on the nanoparticle surface. This step is accompanied by a weak endothermic DTA signal, confirming the loss of physically bound water.

The second gradual weight loss of ~2% between 250–750 °C corresponds to the slow decomposition of the remaining organic biomolecules originating from *Buchanania lanzan Spreng* extract, such as flavonoids, phenolics, and reducing sugars. These biomolecules act as capping and stabilizing agents during nanoparticle formation, and their thermal degradation results in minor exothermic events on the DTA curve.

A major weight loss of ~11% occurring between 800–950 °C is observed in the final stage, which is associated with the complete disintegration of bioorganic constituents that were capped on the surface of the CuO NPs and removal of strongly bound carbonaceous residues. The strong exothermic peak in the DTA curve in this region indicates combustion of these organic remnants and reorganization of the copper oxide lattice.

Beyond 950 °C, no significant mass loss is observed, confirming the formation of thermally stable monoclinic CuO nanoparticles. The relatively low total weight loss further indicates efficient capping and minimal organic contamination, validating the successful synthesis of CuO using the *B. lanzan* leaf extract.[27]

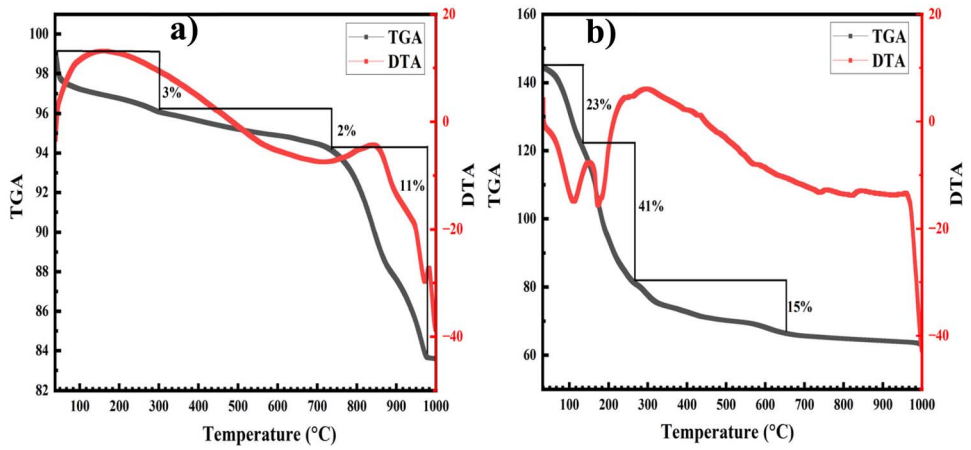

Fig. 8 Comparative TGA-DTA profiles of (a) green CuO and (b) Gel@CuO microspheres showing minor thermal degradation for pure CuO and significant multistep decomposition for Gel@CuO due to the alginate matrix, with CuO remaining as the stable inorganic residue in both cases.

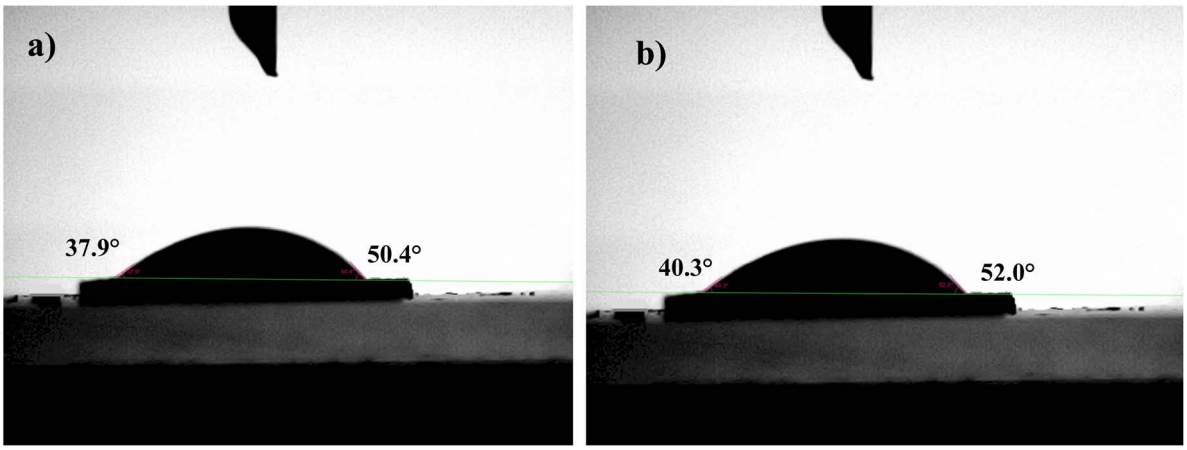

Fig. 9 Contact angle images of Gel@CuO microspheres; (a) shows contact angles of 37.9° and 50.4°, and (b) shows 40.3° and 52.0°.

The thermal behaviour of the Gel@CuO microspheres (Fig. 8b) reveals three major mass-loss regions, corresponding to the removal of absorbed water, degradation of the alginate biopolymer matrix, and final structural stabilization of the CuO-loaded gel network.

The first weight loss of ~23% below 200 °C is attributed to the evaporation of physisorbed and bound water within the hydrogel structure, along with the release of residual solvents trapped during microsphere formation. The accompanying endothermic events in the DTA trace further confirm moisture loss and dehydration of the alginate network. The second and most significant weight loss of ~41% occurring between 200–350 °C corresponds to the thermal decomposition of the sodium alginate backbone. In this temperature region, the glycosidic linkages and polysaccharide chains undergo depolymerisation, decarboxylation, and oxidative degradation. The strong exothermic transitions observed in the DTA curve support combustion of the organic components and breakdown of carboxylate and hydroxyl functionalities that stabilize the CuO nanoparticles within the gel. A third gradual weight loss of ~15% between 350–700 °C reflects the slow removal of carbonaceous char and strongly bound organic residues produced during the earlier decomposition stages. Beyond ~700 °C, the TGA curve becomes nearly stable, indicating that the remaining material predominantly consists of thermally robust inorganic CuO. The final exothermic peak near 1000 °C is associated with the structural rearrangement or crystallite ordering of CuO.

Overall, the TGA-DTA profile confirms that the Gel@CuO microspheres contain a substantial organic fraction from the alginate matrix and that CuO remains as the major thermally stable residue. This behaviour is consistent with the encapsulation of CuO nanoparticles within a biopolymer network, affirming the successful formation of Gel@CuO microspheres.

3.1.3.2 Contact angle study. The wettability of the Gel@CuO microsphere nanocatalyst was assessed using static contact-angle measurements. The geometrical structure and chemical nature of the solid surface, along with its interaction with liquids, govern the wettability, which is expressed in terms of the contact angle (CA). Higher wettability corresponds to lower contact angle values and indicates hydrophilic behavior, whereas higher contact angles reflect hydrophobicity.[28]

Two independent measurements were performed on different regions of the Gel@CuO microsphere surface to evaluate surface uniformity and reproducibility. Fig. 9a and b shows

Table 1 Comparison of reported Petasis reaction conditions with the present Gel@CuO method, showing its advantages in terms of reaction time, mild conditions, and yields

	Experimental conditions					
Entry	Solvent	Catalyst	Temp (°C)	Time	Yield	References
1	Glycerol	—	50 °C	48 h	77	30
2	Ball mining	Neutral alumina, 450 rpm	—	105 min	92	31
3	Glycerol: ChCl	—	80 °C	5 h	95	32
4	Aq 30% NaPTS solution, (((·)))	—	RT	24 min	92	33
5	THF	Natural pozzolan	Reflux	24 h	74	34
6	DCM, MW	—	120 °C (300W)	10 min	76	35
7	Acetonitrile	$CoFe_2O_4$	Reflux	2.5 h	88	36
8	DME	Zn_2Ln_2 clusters	RT	14 h	95	37
9	DCM	Pd–MgAlO	Reflux	4 h	87	38
10	1,4-Dioxane	Trititanate nanotubes (TNT)	60 °C	60 min	93	39
11	Solvent free (MW)	—	120 °C	2 h	78	40
12	**Gel@CuO**	**10% aq. NaPTS hydrotrope**	**50 °C**	**40 min**	**96**	**Present work**

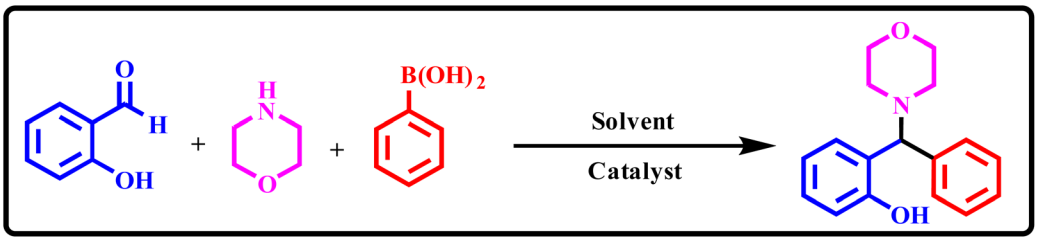

Scheme 2 Gel@CuO catalyzed Petasis reaction in aqueous NaPTS.

Table 2 Screening of different solvents with Gel@CuO for the Petasis reaction

Entry	Solvent (3 mL)	Conditions[a]	Time	Yield
1	DCM	RT	8 h	88
2	DCM	Reflux	5 h	88
3	Toluene	Reflux	11 h	82
4	MeOH	Reflux	9 h	83
5	MeCN	Reflux	10 h	76
6	EtOAc	Reflux	16 h	74
7	$CHCl_3$	Reflux	12 h	78
8	Water	50	24 h	84
9	Water	80	12 h	84
10	Ethanol	Reflux	22 h	86
11	Water + ethanol (9 : 1)	RT	9 h	78
12	**Aq. NaPTS hydrotrope**	**RT**	**9 h**	**86**
13	**Aq. NaPTS hydrotrope**	**50 °C**	**5 h**	**88**
14	**Aq. NaPTS hydrotrope**	**Gel@CuO, 50 °C**	**38 min**	**98**

[a] Reaction conditions: salicyalaldehyde (1 mmol), morpholine (1 mmol), and 4-methoxyphenylboronic acid (1 mmol) in aq. NaPTS (3 mL), catalyst (Gel@CuO), under 50 °C as mentioned above.

the surface contact angles, which are less than 90° which reveals the hydrophilic nature of all of these surfaces.[29] The slight variation in contact angle values between Fig. 9a and b can be attributed to surface roughness and minor heterogeneity within the calcium–alginate matrix. Sodium alginate contains abundant hydrophilic –OH and $–COO^-$ groups; therefore, the native alginate matrix already supports strong water affinity.

The close agreement between the contact-angle values obtained from Fig. 9a (37.9° and 50.4°) and Fig. 9b (40.3° and 52.0°) confirms the uniform distribution of active sites and consistent surface characteristics across the microspheres. Moreover, no evidence of nanoparticle leaching was observed during droplet deposition, indicating strong confinement of CuO within the alginate matrix.

The hydrophilic nature of the Gel@CuO microspheres plays a crucial role in enhancing catalytic performance, particularly in aqueous NaPTS medium. The strong affinity of the catalyst surface toward water facilitates improved dispersion of the catalyst, enhances the adsorption of polar reactants, and promotes efficient mass transfer between the reactants and active sites. This results in better accessibility of catalytic sites and faster reaction kinetics. Overall, the catalyst surface is well-suited for aqueous-phase reactions, supporting its application in green catalytic systems.

3.2 Catalytic properties

Table 1 summarizes the previously reported catalytic systems for the Petasis reaction, highlighting the wide range of solvents, catalysts, and operating conditions employed. Many of these methodologies rely on prolonged reaction times, elevated temperatures, or non-green media, often resulting in only moderate yields. In contrast, our newly developed Gel@CuO catalytic system operates efficiently under mild aqueous hydrotropic conditions (10% NaPTS, 50 °C) and delivers high yields (96%) within 40 Min (Scheme 2). This demonstrates that Gel@CuO serves as a robust and sustainable heterogeneous catalyst for the synthesis of alkylaminophenols, offering a greener and more practical alternative to previously reported approaches. Compared to previously reported systems, the present methodology offers shorter reaction times, milder conditions, and improved sustainability, highlighting its practical applicability.

3.2.1 Optimization of experimental conditions. To identify optimal reaction conditions, a model Petasis reaction between salicylaldehyde (1.0 mmol), morpholine (1.0 mmol), and 4-methoxyphenylboronic acid (1.0 mmol) was selected and carried out in the presence of the Gel@CuO nanocatalyst. Initially, a range of conventional organic solvents, including dichloromethane (DCM), toluene, methanol, acetonitrile, ethyl acetate, chloroform, and ethanol, were screened under both room temperature and reflux conditions (Table 2). While moderate to good yields (74–88%) were obtained in these solvents, the reactions generally required longer reaction times (4–16 h) and, in most cases, elevated temperatures. Subsequently, aqueous systems were investigated. Reactions performed in water at 50 °C and 80 °C afforded moderate yields (84%) but still required extended reaction times (12–24 h), indicating limited efficiency due to the poor solubility of organic substrates, particularly boronic acids. A mixed solvent system (water : ethanol, 9 : 1) also did not significantly improve the reaction outcome.

In contrast, the use of aqueous sodium *p*-toluenesulfonate (NaPTS) as a hydrotropic medium resulted in a notable enhancement in reaction efficiency. At room temperature and 50 °C, the reaction proceeded with improved yields (86–88%) and reduced reaction times (5–9 h). Importantly, under optimized conditions using the Gel@CuO nanocatalyst in aqueous NaPTS at 50 °C, the model reaction was completed within 38 minutes, affording an excellent yield of 98%. This enhanced performance can be attributed to the dual role of NaPTS: it acts

Table 3 Synthesis of alkylaminophenols, aryl glycines, and fused heterocycles under mild conditions

Entry no.	Aldehyde	Amines	Boronic acids	Product[a]	Yield	Time
1	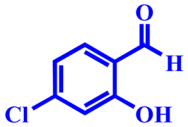 1a	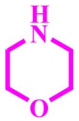 2a	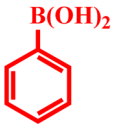 3a	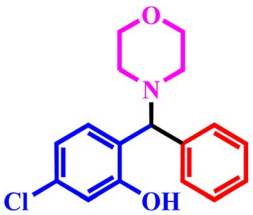 4a	96	55 min
2	1a	2a	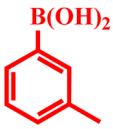 3b	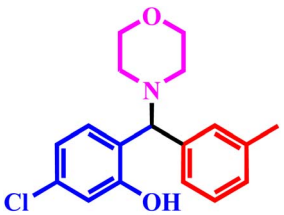 4b	97	52 min
3	1a	2a	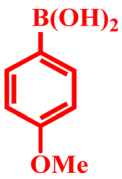 3c	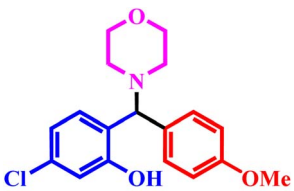 4c	98	40 min
4	1a	2a	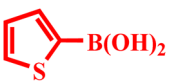 3d	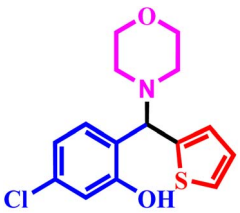 4d	92	52 min
5	1a	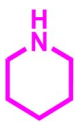 2b	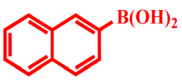 3e	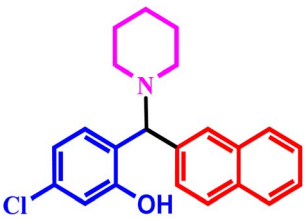 4e	90	54 min
6	1a	2b	3a	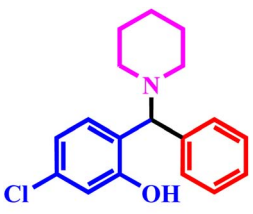 4f	94	42 min

Table 3 (*Contd.*)

Entry no.	Aldehyde	Amines	Boronic acids	Product[a]	Yield	Time
7	**1a**	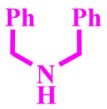 **2c**	**3a**	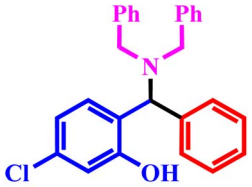 **4g**	98	44 min
8	**1a**	**2c**	**3b**	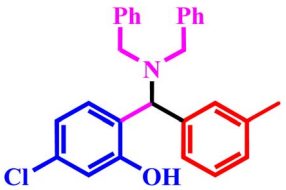 **4h**	96	46 min
9	**1a**	 **2d**	**3b**	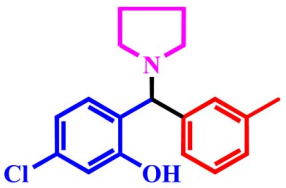 **4i**	96	44 min
10	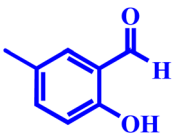 **1b**	**2a**	**3a**	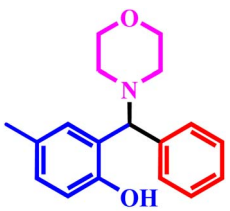 **4j**	95	56 min
11	**1b**	**2b**	**3b**	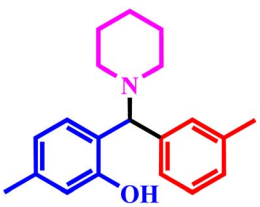 **4k**	94	54 min
12	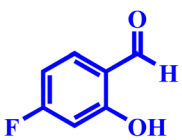 **1c**	**2a**	**3b**	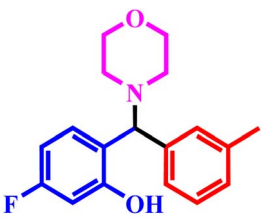 **4l**	96	60 min

Table 3 (*Contd.*)

Entry no.	Aldehyde	Amines	Boronic acids	Product[a]	Yield	Time
13	**1c**	**2a**	**3c**	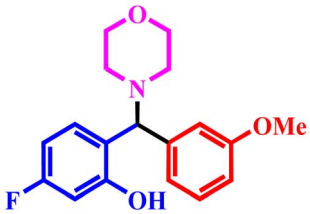 **4m**	96	56 min
14	**1c**	**2b**	**3a**	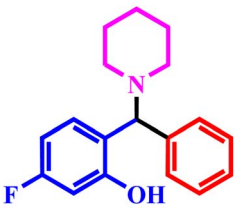 **4n**	94	58 min
15	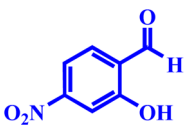 **1d**	**2a**	**3c**	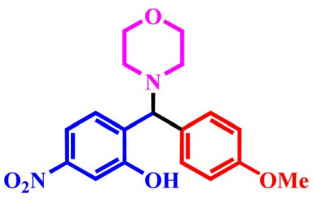 **4o**	94	58 min
16	**1d**	**2b**	**3a**	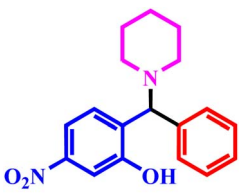 **4p**	88	1.10 h
17	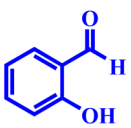 **1e**	**2a**	**3a**	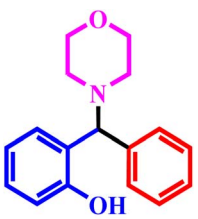 **4q**	96	40 min
18	**1e**	**2a**	**3c**	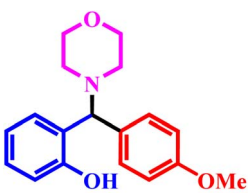 **4r**	98	38 min

Table 3 (*Contd.*)

Entry no.	Aldehyde	Amines	Boronic acids	Product[a]	Yield	Time
19	**1e**	**2b**	**3b**	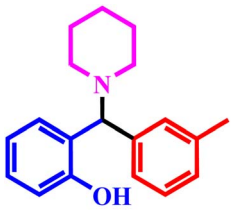 **4s**	96	42 min
20	**1e**	**2b**	**3c**	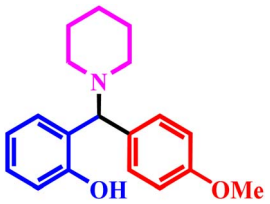 **4t**	97	40 min
21	**1e**	**2c**	**3c**	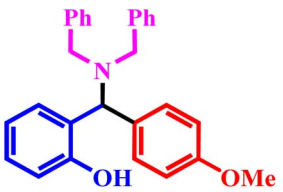 **4u**	98	40 min
22	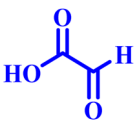 **1f**	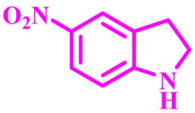 **2e**	**3c**	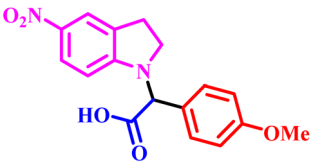 **4v**	98	50 min
23	**1f**	**2e**	**3a**	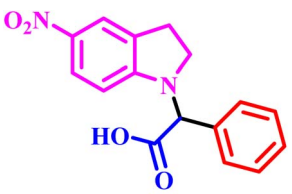 **4w**	96	56 min
24	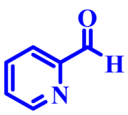 **1g**	**2c**	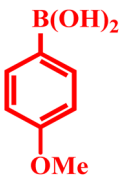	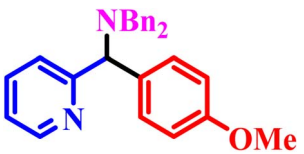 **4x**	86	1.5 h

Table 3 (*Contd.*)

Entry no.	Aldehyde	Amines	Boronic acids	Product[a]	Yield	Time
25	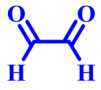 **1h**	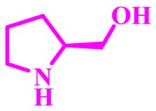 **2f**	**3a**	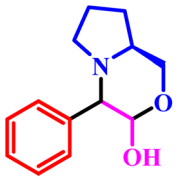 **4y**	92	30 min
26	**1h**	**2f**	**3c**	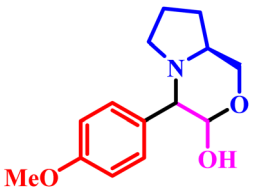 **4z**	98	7 min
27	**1h**	**2f**	**3b**	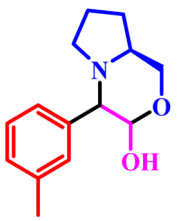 **4Z$_1$**	96	15 min

[a] Reaction conditions: aldehyde (**1a**-1h mmol), **2a**-2f (1 mmol), and **4a–4Z$_1$** (1 mmol) in aq. NaPTS (3 mL), catalyst (Gel@CuO), under 50 °C as mentioned above.

as a hydrotrope to increase the solubility of relatively hydrophobic reactants, particularly boronic acids, in the aqueous medium, thereby facilitating effective interaction with the catalytic sites. Additionally, NaPTS assists in the abstraction (or partial deprotonation) of the phenolic –OH group of salicylaldehyde, increasing its nucleophilicity and promoting coordination with the catalytic center. A control experiment performed in the absence of the Gel@CuO catalyst showed that the reaction required approximately 5 h for completion, whereas in the presence of the catalyst, the reaction was completed within 38 min, confirming the crucial catalytic role of Gel@CuO.

3.2.2 Catalytic efficiency and substrate scope of Gel@CuO. Table 3 demonstrates the broad applicability of the Gel@CuO nanocatalyst in the diverse Petasis transformations, enabling three structurally distinct product classes under different mild aqueous NaPTS conditions (Scheme 3). The substrate scope of the Gel@CuO catalyzed Petasis reaction was systematically explored using a wide range of aldehydes, amines, and boronic acids. Entries 1–16 correspond to substituted alkylaminophenol derivatives synthesized from substituted salicylaldehydes under optimized conditions in 10% aqueous NaPTS at 50 °C. The observed reactivity trend is governed by electronic effects operating during the key phenolic O → Cu → B coordination step, which initiates the Petasis catalytic cycle. Unsubstituted salicylaldehyde (entries 17–21) afforded the highest yields, reflecting optimal phenolic nucleophilicity and efficient boronate complexation. 4-Chloro-2-hydroxybenzaldehyde

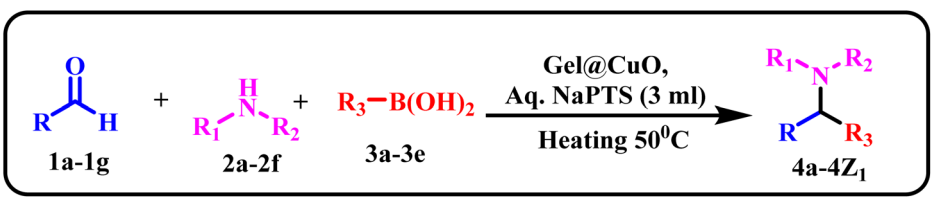

Scheme 3 Gel@CuO catalyzed synthesis of Petasis reaction products (**4a–4Z$_1$**) in aqueous NaPTS at 50 °C.

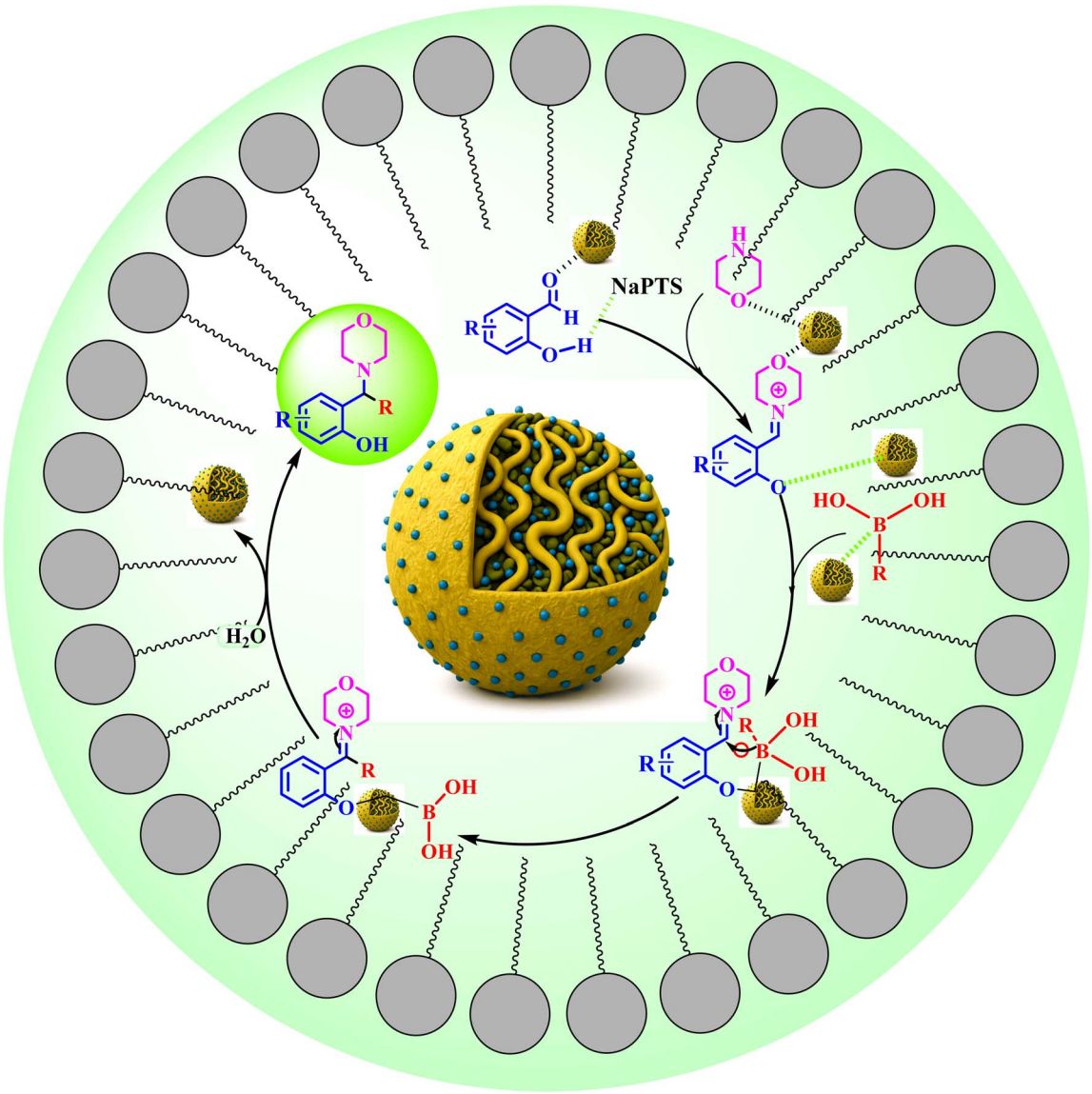

Scheme 4 Plausible mechanism for the synthesis of Petasis reaction products (4a–4Z_1) using Gel@CuO catalyst in aqueous NaPTS at 50 °C.

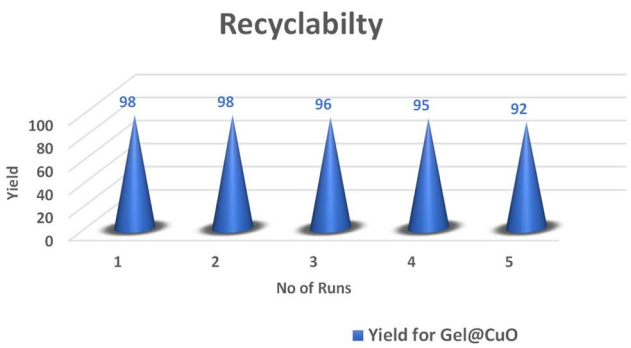

Fig. 10 Recyclability of Gel@CuO microspheres over five cycles, demonstrating high catalytic durability with minimal loss in yield.

derivatives (entries 1–9) provided slightly reduced but still excellent yields due to chlorine's moderate – I effect, which enhances aldehyde electrophilicity without significantly diminishing phenolic oxygen donation. In contrast, 4-fluoro and 4-nitro salicylaldehyde derivatives (entries 12–16) exhibited comparatively lower conversions, as strongly electron-withdrawing substituents decrease electron density on the phenolic oxygen, weakening boronate formation and slowing aryl migration. Across this series, electron-rich boronic acids consistently delivered superior yields, in agreement with their enhanced migratory aptitude in the B → C aryl transfer step.

Entries 22–23 describe the formation of indoline-derived aryl-glycine analogues using glyoxylic acid as the aldehydic component. These transformations required a higher hydrotropic strength and proceeded efficiently in 30% aqueous NaPTS, which improves the solubilization of the highly polar glyoxylic acid and stabilises the iminium intermediate. Once again, 4-methoxyphenylboronic acid outperformed phenylboronic acid, reinforcing the role of electron donation in accelerating the aryl migration step.

Table 4 Zone of inhibition of 1-plant extract, 2-CuO NPs, 3-sodium alginate, 4-CuO NPs + sodium alginate, 5-antibiotic and C-control antimicrobial activity against human pathogenic strains

	Antibacterial activity			
	Gram +ve		Gram −ve	
Entry	*Staphylococcus aureus* (NCIM-2654)	*Bacillus cereus* (NCIM-2703)	*Salmonella typhimurium* (NCIM-2501)	*Proteus vulgaris* (NCIM-2813)
1-PE	10.67 ± 0.58	11.67 ± 0.58	10.33 ± 0.58	11.87 ± 0.23
2-CuO NPs	16.33 ± 0.58	21.67 ± 0.58	20.33 ± 0.58	21.00 ± 1.00
3-SA	10.00 ± 1.00	10.67 ± 0.58	10.33 ± 0.58	10.33 ± 0.58
4-CuO NPs + SA	15.67 ± 0.58	20.67 ± 0.58	14.33 ± 0.58	13.67 ± 0.58
5-Ab	25.33 ± 0.58	20.67 ± 1.15	24.00 ± 1.00	27.67 ± 0.58

Finally, entries 25–27 demonstrate the synthesis of fused morpholine–pyrrolidine frameworks *via* Petasis coupling of glyoxal with cyclic amino alcohols such as pyrrolidin-2-ylmethanol and (*S*)-piperidin-2-ylmethanol. These reactions proceeded smoothly in 10% NaPTS, indicating that lower hydrotrope concentrations are sufficient for these intrinsically polar substrates. Remarkably, entry 27 achieved a 98% yield within only 7 min, significantly faster than all other transformations, suggesting a highly favourable electronic and steric environment that accelerates iminium formation and boronate collapse. Overall, the high efficiency, short reaction times, and broad substrate tolerance highlight the synergistic role of CuO Lewis acidic sites and the hydrophilic alginate matrix, which together enhance mass transfer, substrate organization, and stabilization of key reaction intermediates within the Gel@CuO microsphere nanocatalyst.

3.2.3 Mechanism. The catalytic cycle begins with activation of the carbonyl compound through coordination with the surface-exposed Cu^{2+} Lewis acidic sites present on the Gel@CuO microspheres, as shown in Scheme 4. Simultaneously, the aqueous sodium *p*-toluenesulfonate (NaPTS) hydrotropic medium plays a crucial role in enhancing the reaction efficiency. NaPTS improves the solubility of relatively hydrophobic reactants, particularly aryl boronic acids, in the aqueous medium through hydrotropic aggregation, thereby facilitating effective interaction among the reactants and the catalyst. In the initial step, the aldehyde reacts with the amine to form an iminium ion intermediate, the formation of which is facilitated by polarization of the carbonyl group through coordination with Cu^{2+} Lewis acidic sites. In the case of salicylaldehyde derivatives, NaPTS further promotes partial deprotonation of the phenolic –OH group, thereby enhancing its nucleophilicity and facilitating its coordination with the Cu^{2+} catalytic center.[41] This interaction stabilizes the iminium intermediate through intramolecular coordination. Subsequently, the activated boronic acid, whose solubility is enhanced by the NaPTS hydrotropic environment, coordinates with CuO that activates the iminium intermediate and facilitates the migration of the aryl/alkyl group from the boronic acid.[5] This step leads to the formation of the alkylaminophenol (or related Petasis product) while simultaneously regenerating the active Cu^{2+} catalytic sites on the Gel@CuO surface.

The alginate matrix further contributes by preventing CuO nanoparticle aggregation, maintaining high dispersion of active sites, and facilitating efficient mass transfer within the aqueous medium. Thus, the synergistic action of CuO Lewis acidity, the hydrophilic alginate network, and the hydrotropic NaPTS medium collectively stabilizes the reaction intermediates, lowers the activation barrier, and enables efficient Petasis multicomponent reactions under mild and environmentally benign conditions.

3.2.4 Recyclability and stability of catalyst. The recyclability of the Gel@CuO nanocatalyst was evaluated for five consecutive cycles using the model Petasis reaction under optimized conditions. As shown in Fig. 10, the catalyst maintained excellent activity, with only a marginal decrease in yield from 98% (1st run) to 92% (5th run). The slight reduction in catalytic efficiency after multiple cycles can be attributed to minor CuO surface passivation, partial pore blockage, or loss of microsphere mass during recovery and washing. Importantly, the overall high yields across repeated runs confirm the robust structural integrity, strong CuO immobilization within the alginate matrix, and minimal metal leaching. These results highlight the efficiency and durability of Gel@CuO as a practical, reusable, and environmentally friendly heterogeneous catalyst suitable for sustainable Petasis transformations.

3.3 Antimicrobial activity

3.3.1 The antimicrobial effect of green-synthesized CuO NPs and Gel@CuO nanocatalyst. The antimicrobial activity of synthesized material was checked along with blank dimethyl sulfoxide (DMSO) as a negative control. The antimicrobial potential of synthesized material and plant extract was studied using the agar well gel diffusion method against bacterial strains *S. aureus*, *B. cereus,* Gram-positive and *S. typhimurium*, *P. vulgaris,* Gram-negative bacteria, using streptomycin as the standard antibiotic drug. The results revealed that the synthesized materials effectively inhibit the growth of all tested bacterial strains. Among them, Gel@CuO nanocatalyst exhibited significantly enhanced antibacterial activity compared to the plant extract and sodium alginate alone. This indicates that the antibacterial activity mainly arises from the presence of CuO nanoparticles. The above data represent the mean ± standard error of three replicates.

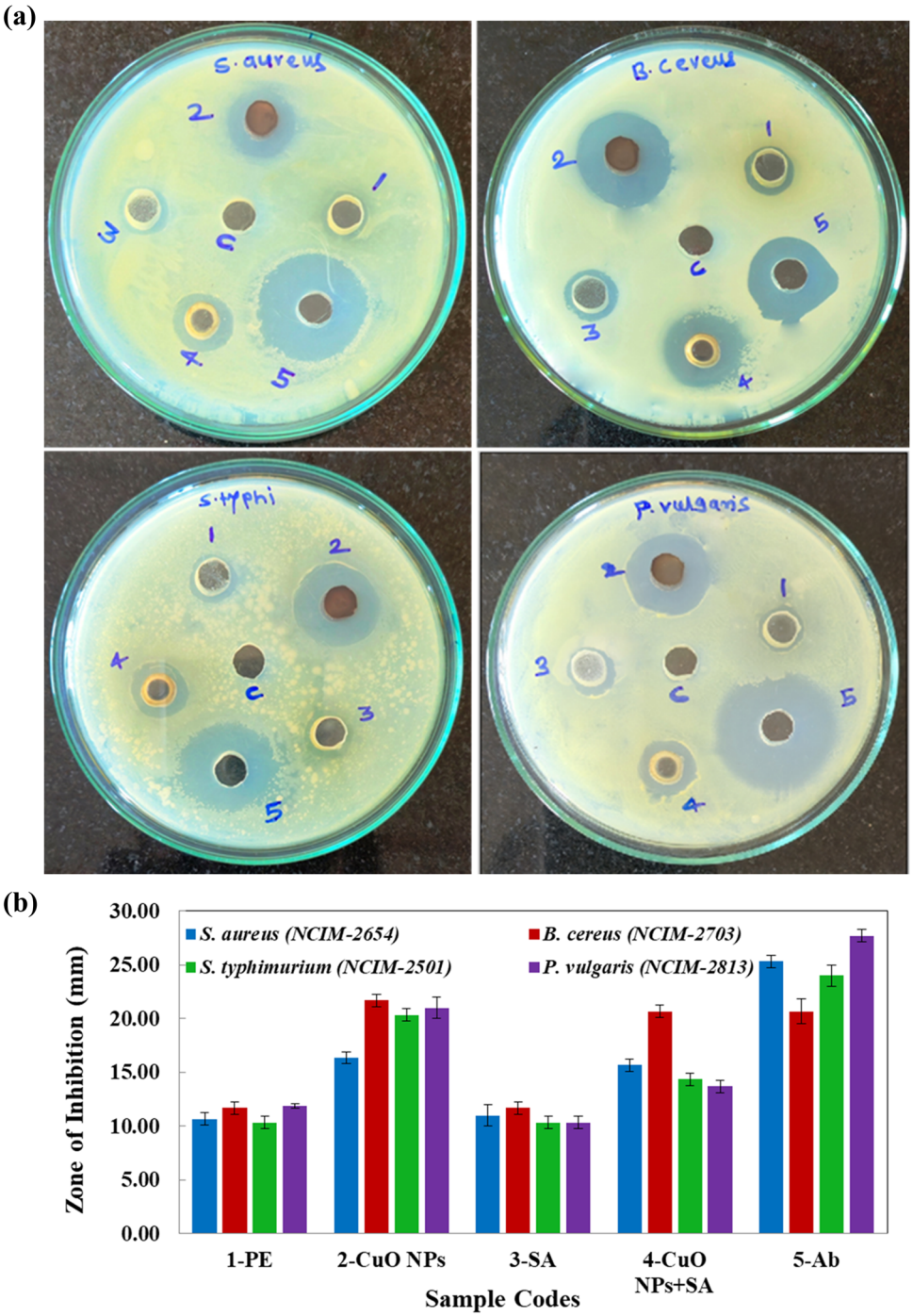

Fig. 11 (a) Antimicrobial activity of 1-plant extract, 2-CuO NPs, 3-sodium Alginate, 4-CuO NPs + sodium alginate (Gel@CuO), 5-antibiotic and C-control on the *Staphylococcus aureus* (NCIM-2654), *Bacillus cereus* (NCIM 2703), *Salmonella typhimurium* (NCIM-2501) and *Proteus vulgaris* (NCIM – 2813) with zone of inhibition. (b) Zone of inhibition of 1-plant extract, 2-CuO NPs, 3-sodium alginate, 4-CuO NPs + sodium alginate, 5-antibiotic and C-control antimicrobial activity against human pathogenic strains.

The antibacterial results (Table 4 and Fig. 11a, b) show that the Gel@CuO microsphere system exhibits significantly improved antibacterial activity compared with the plant extract (1-PE) and sodium alginate alone (3-SA). Sodium alginate itself displays very weak antibacterial activity, as reflected by the small inhibition zones (~10–11 mm), indicating that the polymer matrix is largely inert toward bacterial growth. The incorporation of CuO nanoparticles into the alginate network leads to a clear increase in antibacterial performance, confirming that the antimicrobial activity mainly originates from the CuO nanoparticles present in the catalytic system. Compared with free green-synthesized CuO nanoparticles (2-CuO NPs), the Gel@CuO nanocatalyst shows slightly lower inhibition zones. This difference may be attributed to partial

encapsulation of CuO nanoparticles within the alginate matrix, which may limit the accessibility of some surface-active sites. However, it should be noted that the antibacterial comparison presented here is qualitative, as the Cu content was not independently standardized between the two systems. Nevertheless, the observed antibacterial activity of Gel@CuO indicates that a sufficient fraction of CuO nanoparticles remains exposed or accessible at the surface of the alginate microspheres, allowing effective interaction with bacterial cells while the alginate framework provides structural stability to the catalyst.

4 Conclusion

This study demonstrates that sodium alginate-derived Gel@CuO microspheres constitute an effective and sustainable heterogeneous nanocatalyst for Petasis multicomponent reactions in aqueous media. The successful biogenic synthesis of CuO nanoparticles (11.82 nm) using *Buchanania lanzan Spreng* leaf extract, followed by their immobilization within a calcium-crosslinked alginate network, resulted in stable, hydrophilic microspheres with accessible active sites. Detailed physicochemical analyses confirmed the preservation of phase-pure monoclinic CuO with an average crystallite size of 11.82 nm, along with strong metal–polymer interactions, homogeneous elemental distribution, and favorable surface wettability, all of which are essential for efficient catalysis under green conditions. The Gel@CuO nanocatalyst exhibited broad substrate compatibility, enabling the synthesis of alkylaminophenols, aryl-glycines, pyridyl derivatives, and fused heterocycles with consistently high yields and short reaction times. Importantly, the catalyst maintained high activity over multiple reuse cycles, confirming its mechanical integrity and resistance to CuO leaching. Quantitative green chemistry metrics further validated the environmental advantage of this protocol, as evidenced by low PMI values, high reaction mass efficiency, and favorable atom economy across diverse product classes. In addition to its catalytic performance, Gel@CuO microspheres displayed notable antibacterial activity, exceeding that of sodium alginate alone, which highlights the functional contribution of surface-exposed CuO nanoparticles. Collectively, these findings establish Gel@CuO microspheres as a multifunctional, eco-compatible catalytic platform that integrates renewable materials, green synthesis, and hydrotropic reaction engineering, offering significant potential for sustainable multicomponent organic transformations.

Conflicts of interest

There are no conflicts to declare.

Data availability

All data supporting this study are included in the article and the supplementary information (SI). Additional data are available from the corresponding author upon reasonable request. Supplementary information is available. See DOI: https://doi.org/10.1039/d6ra00921b.

References

1 T. Ghosh, S. S. Ahamed, R. Paul and P. Saha, Employing Multicomponent Reactions in Heterocycle Synthesis: Recent Advances, *Eur. J. Org Chem.*, 2025, **28**(35), e202500337, DOI: 10.1002/ejoc.202500337.
2 V. Kasi, M. EI Sayed Abdelsalam Zaki, H. B. Nabisahebgari, H. Shaik, S.-K. Chang, L. S. Wong, K. Parasuraman and S. M. Gomha, Magnetic Nanoparticle-Catalysed One-Pot Multicomponent Reactions (MCRs): A Green Chemistry Approach, *Catalysts*, 2025, **15**(9), 800.
3 P. Wu, M. Givskov and T. E. Nielsen, Reactivity and Synthetic Applications of Multicomponent Petasis Reactions, *Chem. Rev.*, 2019, **119**(20), 11245–11290, DOI: 10.1021/acs.chemrev.9b00214.
4 N. T. Pandit and S. B. Kamble, The Petasis Reaction: Applications and Organic Synthesis—A Comprehensive Review, *Top. Curr. Chem.*, 2025, **383**(1), 7, DOI: 10.1007/s41061-025-00491-2.
5 N. Pandit, A. Kadam, A. Survase, P. Ashara, A. Patil, C. Bagade, S. Patil and S. Kamble, Phyto-Engineered Pd-Doped WO_3 Nanocomposite *via Anisomeles Indica* Leaf Extract: A Recyclable Heterogeneous Catalyst for Aqueous Petasis Reaction, Photocatalytic Dye Degradation, and Antibacterial Applications, *RSC Adv.*, 2025, **15**(49), 41995–42008, DOI: 10.1039/D5RA06905J.
6 N. T. Pandit, A. D. Kadam, A. A. Survase, V. B. Ghanwat, N. S. Dhane, P. M. Shah and S. B. Kamble, Co-Engineered Ag/CuO Nanoparticles *Via* Artemisia Pallens: Catalytic, Antibacterial, and Molecular Docking Perspectives, *J. Cluster Sci.*, 2025, **36**(6), 198, DOI: 10.1007/s10876-025-02911-1.
7 J. Wang, B. Xu, S. Si, H. Li and G. Song, A Simple and Efficient Synthesis of Fused Morpholine Pyrrolidines/Piperdines with Potential Insecticidal Activities, *Mol. Divers.*, 2014, **18**(4), 887–893, DOI: 10.1007/s11030-014-9531-9.
8 Y. Li and M.-H. Xu, Lewis Acid Promoted Highly Diastereoselective Petasis Borono-Mannich Reaction: Efficient Synthesis of Optically Active β,γ-Unsaturated α-Amino Acids, *Org. Lett.*, 2012, **14**(8), 2062–2065, DOI: 10.1021/ol300581n.
9 J. Singh, G. Kaur and M. Rawat, A Brief Review on Synthesis and Characterization of Copper Oxide Nanoparticles and Its Applications, *J. Bioelectron. Nanotechnol.*, 2016, **1**, 9.
10 A. Banger, A. Kumari, N. K. Jangid, S. Jadoun, A. Srivastava and M. Srivastava, A Review on Green Synthesis and Characterisation of Copper Nanoparticles Using Plant Extracts for Biological Applications, *Environ. Technol. Rev.*, 2025, **14**(1), 94–126, DOI: 10.1080/21622515.2025.2453950.
11 A. Kadam, A. Survase and S. Kamble, Biosynthesis of Copper Nanoparticles Using Aqueous Pisa Plant Leaf Extracts: Antimicrobial Activities and Catalytic Application for Xanthene Synthesis, *ChemistrySelect*, 2023, **8**(45), e202303777.

12 M. V. Samadhan, *Studies on Seed Germination in Charoli (Buchanania Lanzan Spreng)*, PhD thesis, Dr Panjabrao Deshmukh Krishi Vidyapeeth, 2019, https://krishikosh.egranth.ac.in/server/api/core/bitstreams/3d680852-8687-4a54-b4ee-f21b4d5f63fb/content, accessed 2025-12-04.
13 P. Jatav and R. K. Tenguria, *Qualitative Analysis of Phytoconstituents of Buchanania Lanzan Leaf Extracts*, 2023.
14 P. S. Pranoti Shirke, L. P. Laxmikant Purane and R. B. Rupali Bhoite, Review on Buchanania Lanzan Phytochemistry, Traditional Used and Pharmacological Potential, *Int. J. Pharm. Res.*, 2025, **10**(3), 89–94, DOI: 10.35629/4494-10038994.
15 A. Purohit, R. Sharma, R. Shiv Ramakrishnan, S. Sharma, A. Kumar, D. Jain, H. S. Kushwaha and E. Maharjan, Biogenic Synthesis of Silver Nanoparticles (AgNPs) Using Aqueous Leaf Extract of Buchanania Lanzan Spreng and Evaluation of Their Antifungal Activity against Phytopathogenic Fungi, *Bioinorg. Chem. Appl.*, 2022, 6825150, DOI: 10.1155/2022/6825150.
16 S. Zeng, X. Jin, D. Rajarathnam and Z. Chen, Enhanced Degradation of Malachite by Iron Nanoparticles Encapsulated in Sodium Alginate Beads, *J. Ind. Eng. Chem.*, 2019, **77**, 238–242.
17 Y. Wang, Z. Shen, H. Wang, Z. Song, D. Yu, G. Li, X. Liu and W. Liu, Progress in Research on Metal Ion Crosslinking Alginate-Based Gels, *Gels*, 2025, **11**(1), 16, DOI: 10.3390/gels11010016.
18 I. Donati and B. E. Christensen, Alginate-Metal Cation Interactions: Macromolecular Approach, *Carbohydr. Polym.*, 2023, **321**, 121280, DOI: 10.1016/j.carbpol.2023.121280.
19 A. N. Bezbaruah, S. Krajangpan, B. J. Chisholm, E. Khan and J. J. Elorza Bermudez, Entrapment of Iron Nanoparticles in Calcium Alginate Beads for Groundwater Remediation Applications, *J. Hazard. Mater.*, 2009, **166**(2–3), 1339–1343, DOI: 10.1016/j.jhazmat.2008.12.054.
20 S. R. Attar, A. C. Sapkal, C. S. Bagade, S. H. Mujawar and S. B. Kamble, Gel Entrapped ZnO Nanorods: An Efficient and Sustainable Catalyst for the Claisen-Schmidt Condensation Reaction in Aqueous Hydrotropic Media, *Mol. Catal.*, 2023, **542**, 113120, DOI: 10.1016/j.mcat.2023.113120.
21 M. Il Kim, C. Y. Park, J. M. Seo, K. S. Kang, K. S. Park, J. Kang, K. S. Hong, Y. Choi, S. Y. Lee, J. P. Park, H. G. Park and T. J. Park, *In Situ* Biosynthesis of a Metal Nanoparticle Encapsulated in Alginate Gel for Imageable Drug-Delivery System, *ACS Appl. Mater. Interfaces*, 2021, **13**(31), 36697–36708, DOI: 10.1021/acsami.1c02286.
22 A. C. Sapkal, S. R. Attar, N. S. Dhane, N. T. Pandit and S. B. Kamble, Green and Eco-Compatible Synthesis of Quinoxaline Molecules Using Chitosan as a Biodegradable Catalyst in Aqueous Hydrotropic Medium, *Tetrahedron*, 2025, **173**, 134456.
23 A. N. Bezbaruah, S. Krajangpan, B. J. Chisholm, E. Khan and J. J. Elorza Bermudez, Entrapment of Iron Nanoparticles in Calcium Alginate Beads for Groundwater Remediation Applications, *J. Hazard. Mater.*, 2009, **166**(2–3), 1339–1343, DOI: 10.1016/j.jhazmat.2008.12.054.
24 N. Dhumal, S. Mangle, M. Kharde, A. Survase, D. Mali and R. Hangarge, Design And Synthesis Of Novel Methylene Bridged Quinoline-1, 2, 3, 4-Tetrahydroisoquinolines As An Antimicrobial Agent, *J. Indian Chem. Soc.*, 2025, 102287.
25 M. Kuczajowska-Zadrożna, U. Filipkowska and T. Jóźwiak, Adsorption of Cu (II) and Cd (II) from Aqueous Solutions by Chitosan Immobilized in Alginate Beads, *J. Environ. Chem. Eng.*, 2020, **8**(4), 103878, DOI: 10.1016/j.jece.2020.103878.
26 S. Paramasivam, S. Chidambaram, P. Karumalaiyan, G. Velayutham, M. Chinnasamy, R. Pitchaipillai and K. J. S. Kumar, Phytogenic Synthesis of Cuprous and Cupric Oxide Nanoparticles Using Black Jack Leaf Extract: Antibacterial Effects and Their Computational Docking Insights, *Antibiotics*, 2024, **13**(11), 1–13, DOI: 10.3390/antibiotics13111088.
27 H. T. Gebrie, M. A. Assege, D. S. Meshesha, B. A. Tebeje, G. W. Moges, A. T. Wodajo, G. M. Manahelohe and A. A. Belew, Biosynthesis and Characterization of Copper Oxide Nanoparticles from Plumbago Zeylanica Leaf Extract for Antibacterial and Antioxidant Activities, *Sci. Rep.*, 2025, **15**(1), 30656, DOI: 10.1038/s41598-025-10700-z.
28 T. S. Bhat, A. S. Kalekar, D. S. Dalavi, C. C. Revadekar, A. C. Khot, T. D. Dongale and P. S. Patil, Hydrothermal Synthesis of Nanoporous Lead Selenide Thin Films: Photoelectrochemical and Resistive Switching Memory Applications, *J. Mater. Sci. Mater. Electron.*, 2019, **30**(19), 17725–17734, DOI: 10.1007/s10854-019-02122-1.
29 P. A. Koyale, S. P. Kulkarni, J. L. Gunjakar, T. D. Dongale, S. S. Sutar, S. S. Soni, Y. G. Kapdi, R. N. R, S. V. Mulik and S. D. Delekar, ZnO Nanorod/Multiwalled Carbon Nanotube Composites Sensitized with Cu-Based Metal–Organic Frameworks as Photoanodes for Solar-Driven Water Splitting, *ACS Appl. Nano Mater.*, 2024, **7**(3), 2662–2674, DOI: 10.1021/acsanm.3c04694.
30 T. Rosholm, P. M. P. Gois, R. Franzen and N. R. Candeias, Glycerol as an Efficient Medium for the Petasis Borono–Mannich Reaction, *ChemistryOpen*, 2015, **4**(1), 39–46, DOI: 10.1002/open.201402066.
31 R. Hosseinzadeh, Z. Lasemi, M. Oloub and M. Pooryousef, A Green Protocol for the One-Pot Multicomponent Petasis Boronic Mannich Reaction Using Ball Milling, *J. Iran. Chem. Soc.*, 2017, **14**(2), 347–355, DOI: 10.1007/s13738-016-0983-y.
32 N. Azizi and E. Farhadi, Straightforward and Rapid Petasis Multicomponent Reactions in Deep Eutectic Solvent, *Curr. Res. Green Sustain. Chem.*, 2021, **4**, 100220, DOI: 10.1016/j.crgsc.2021.100220.
33 N. T. Pandit, A. D. Kadam, S. S. Ghutukade, A. B. Ghode and S. B. Kamble, Ultra-Probe Assisted Petasis Reaction in Aqueous Hydrotropic Medium: A Green and Sustainable Approach for Alkylaminophenol Synthesis with Molecular Docking Studies, *J. Indian Chem. Soc.*, 2025, **102**(8), 101839, DOI: 10.1016/j.jics.2025.101839.

34 M. Boukachabia, H. Bendjeffal, T. Bouaroudj, A. Djebli and O. Riant, Natural Pozzolan as a Novel Heterogeneous Catalyst for the Synthesis of Alkylaminophenols, *J. Organomet. Chem.*, 2025, **1033**, 123635.

35 N. J. McLean, H. Tye and M. Whittaker, Microwave Assisted Petasis Boronic-Mannich Reactions, *Tetrahedron Lett.*, 2004, **45**(5), 993–995, DOI: 10.1016/j.tetlet.2003.11.092.

36 A. M. Kulkarni, K. S. Pandit, P. V. Chavan, U. V. Desai and P. P. Wadgaonkar, Cobalt Ferrite Nanoparticles: A Magnetically Separable and Reusable Catalyst for Petasis-Borono–Mannich Reaction, *RSC Adv.*, 2015, **5**(86), 70586–70594, DOI: 10.1039/c5ra10693a.

37 P. Kumar, K. Griffiths, S. Lymperopoulou and G. E. Kostakis, Tetranuclear Zn_2Ln_2 Coordination Clusters as Catalysts in the Petasis Borono-Mannich Multicomponent Reaction, *RSC Adv.*, 2016, **6**(82), 79180–79184, DOI: 10.1039/c6ra17209a.

38 A. Fodor, Z. Hell and L. Pirault-Roy, Catalytic Activity of Metal-Doped Porous Materials in the Salicylaldehyde Petasis-Borono Mannich Reaction, *Monatsh. Chem.*, 2016, **147**(4), 749–753, DOI: 10.1007/s00706-016-1681-2.

39 B. R. Prasad Reddy, P. V. Govardhana Reddy, D. P. Kumar, B. N. Reddy and M. V. Shankar, Rapid Synthesis of Alkylaminophenols *via* the Petasis Borono–Mannich Reaction Using Protonated Trititanate Nanotubes as Robust Solid–Acid Catalysts, *RSC Adv.*, 2016, **6**(18), 14682–14691, DOI: 10.1039/c5ra25064a.

40 F. Lamaty, P. Nun and J. Martinez, Microwave-Assisted Neat Procedure for the Petasis Reaction, *Synthesis*, 2010, **2010**(12), 2063–2068, DOI: 10.1055/s-0029-1218727.

41 S. Patil, N. Pandit, A. Kadam, S. Attar, C. Bagade, D. Pore and S. Kamble, A Novel Nanocatalyst Praseodymium Oxide (Pr_6O_{11}) for the Efficient and Sustainable Synthesis of Chromene Derivatives *via* Ultrasound Irradiation in an Aqueous Hydrotropic Medium, *RSC Adv.*, 2025, **15**(32), 25985–25999.